ACS APPLIED MATERIALS & INTERFACES

Research Article

www.acsami.org

Au Nanostructured Surfaces for Electrochemical and Localized Surface Plasmon Resonance-Based Monitoring of α-Synuclein−Small Molecule Interactions

Xin R. Cheng,[†] Gregory Q. Wallace,[‡] François Lagugné-Labarthet,[‡] and Kagan Kerman*,[†]

[†]Department of Physical and Environmental Sciences, University of Toronto Scarborough, Toronto, Ontario M1C 1A4, Canada

[‡]Department of Chemistry, University of Western Ontario, London, Ontario N6A 5B7, Canada

Supporting Information

ABSTRACT: In this proof-of-concept study, the fabrication of novel Au nanostructured indium tin oxide (Au-ITO) surfaces is described for the development of a dual-detection platform with electrochemical and localized surface plasmon resonance (LSPR)-based biosensing capabilities. Nanosphere lithography (NSL) was applied to fabricate Au-ITO surfaces. Oligomers of α-synuclein (αS) were covalently immobilized to determine the electrochemical and LSPR characteristics of the protein. Cyclic voltammetry (CV) and differential pulse voltammetry (DPV) were performed using the redox probe $[Fe(CN)_6]^{3-/4-}$ to detect the binding of Cu(II) ions and (−)-epigallocatechin-3-gallate (EGCG) to αS on the Au-ITO surface. Electrochemical and LSPR data were complemented by Thioflavin-T (ThT) fluorescence, surface plasmon resonance imaging (SPRi), and transmission electron microscopy (TEM) studies. EGCG was shown to induce the formation of amorphous aggregates that decreased the electrochemical signals. However, the binding of EGCG with αS increased the LSPR absorption band with a bathochromic shift of 10−15 nm. The binding of Cu(II) to αS enhanced the DPV peak current intensity. NSL fabricated Au-ITO surfaces provide a promising dual-detection platform to monitor the interaction of small molecules with proteins using electrochemistry and LSPR.

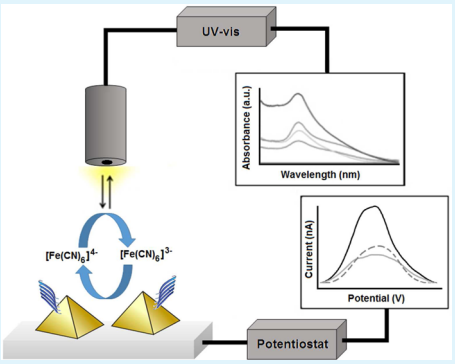

KEYWORDS: *α-synuclein, Parkinson's disease, electrochemistry, biosensor, nanosphere lithography*

INTRODUCTION

Nanosphere lithography (NSL) is a low-cost nanofabrication technique capable of producing well-ordered 2D arrays of periodic nanostructures over large surfaces.[1] NSL has also been applied for the synthesis of size-tunable noble metal nanoparticles organized onto surfaces.[2−5] This characteristic of NSL has been especially valuable for investigating the size-dependent optical properties toward the development of chemical and biological nanosensors.

In general, NSL makes use of transferring a monolayer of nano- or microspheres onto a surface forming a tightly packed pattern, which is ultimately used as a mask for pattern transfer. By removing the spheres after metal thin film deposition, the remaining 2-D nanostructures on the substrate displays nanoscale triangular or pyramidal features arranged in a hexagonal pattern. Au and Ag nanopyramid and nanotriangle arrays, that were prepared using NSL, have been extensively characterized using extinction measurements to identify the dipolar and quadrupolar resonances of the localized surface plasmon (LSPR)[2] while surface-enhanced Raman spectroscopy (SERS) was demonstrated on platforms functionalized with organic molecules.[4,6−9] LSPR occurs when the free electrons of noble metal nanoparticles resonate in response to an optical excitation. Similar to SPR detection, LSPR sensors respond to refractive index changes on nanostructures. However, unlike SPR sensors, these nanostructured sensors usually utilize straight light coupling and do not require complex optical path coupling like Kretschmann configuration. Thus, such simplicity and miniaturization of the light path make LSPR sensors promising platforms for measuring local refractive index changes caused by the adsorption of target molecules. The figure of merit (FOM) values, which are refractive index sensitivities divided by plasmon resonance line widths, of LSPR sensors are usually used to determine the performance of these sensors. Due to radiative damping, which broadens the resonance peaks, the FOM of LSPR sensors are usually a couple orders of magnitude smaller compared to conventional SPRs.[10,11] One way to optimize FOM of LSPR sensors is to decrease the plasmonic full width at half-maximum (fwhm) of the LSPR. This could be done by patterning metal nanoparticles into two-dimensional arrays.[12−15] The resonance wavelength of such NSL platforms can be finely tuned by modifying the chemical nature of the material as well as the geometric parameters of the individual structure. Once the excitation wavelength matches the LSPR of the metallic nanostructure, a large enhancement of the confined electro-

Received: November 13, 2014
Accepted: January 26, 2015
Published: January 26, 2015

DOI: 10.1021/am507972b
ACS Appl. Mater. Interfaces 2015, 7, 4081−4088

magnetic field can be used to detect molecules located in its vicinity. It is known that the uniformity of Au nanostructures on surfaces as well as the opto-geometric parameters of the metallic structures are critical and ultimately affect the width and the position of the LSPR bands as well as the sensitivity of the optical measurements.[16,17] It has also been recently reported that materials having sharp corners and edges provide larger LSPR excitation and red-shift in comparison to their spherical counterparts.[18] A single layer NSL mask could create such a periodic sharp-edged particle array in a highly cost-effective and simple manner when compared with other lithography methods such as nanoimprint lithography, deep UV lithography, X-ray lithography, electron beam lithography, scanning probe lithography, etc.[19] Recently, electrochemistry and LSPR have been utilized on the same platform for the detection of biomolecular interaction,[20,21] but the nanostructure fabrication techniques were often limited by their complexity, cost, and/or the need of a prepatterned structure. To the best of our knowledge, this is the first report about the application of NSL-based Au nanostructured indium tin oxide (Au-ITO) surfaces for the electrochemical and LSPR-based detection of small molecule−protein interactions.

Parkinson's disease (PD) is the second most common neurodegenerative disorder in the world after Alzheimer's disease (AD).[22] PD is more common in the elderly, and it imposes a significant social and economic burden on society.[23] It is pathologically characterized by a loss of dopaminergic neurons in the substantia nigra and aggregated α-synuclein (αS) protein deposits in the peripheral of intraneuronal inclusions called Lewy bodies.[24−26] Several studies have shown that αS misfolding and its dysfunctional regulation in Lewy bodies are key factors in the pathogenesis of PD.[27−31] Oligomers of αS are viewed as the neurotoxic species that are responsible for neuronal death in the early stages of PD.[32] There is compelling evidence that the loss of transition metal homeostasis results in oxidative stress and toxicity in PD.[30] Such toxicity has been shown to be caused by αS oligomers that have undergone morphological changes in the presence of metal ions.[32] In particular, αS was reported to bind strongly to the Cu(II) ions.[33−35] Cu(II) was found highly effective in inducing αS aggregation.[36] Circular dichroism analysis of the interaction between Cu(II) and αS suggested an increase in helical content.[37] Structural studies based on nanoelectron-spray ionization mass spectrometry also showed that Cu(II) induced the formation of highly compact fibrils of αS at pH 7.4.[38]

On the other hand, (−)-epigallocatechin-3-gallate (EGCG), a green tea polyphenol, has been found to possess antiamyloidogenic properties.[39−43] It has been shown to inhibit the misfolding of both αS and amyloid-β (Aβ) (protein associated with the progression of AD) by directly binding and preventing their conversion into toxic aggregates. Instead of β-sheet-rich amyloid fibrils, nontoxic and unstructured forms of αS and Aβ were promoted in the presence of EGCG. Mechanistic studies revealed that EGCG mediated the amyloid conformational change without their disassembly into monomers or small diffusible oligomers.[44]

Due to the hypothesis that there may be independent, competing aggregation pathways in amyloidogenic proteins that can be specifically targeted with chemical compounds, the effects of these small molecules on amyloid aggregation have been of great interest to researchers.[45−48] These antiamyloidogenic compounds have been extensively studied using fluorescence spectroscopy,[49] electron microscopy,[50] or SPR.[45] Many of these techniques require labeling and expensive instrumentation. Our group has previously reported the label-free detection of aggregation in Aβ and αS by monitoring the electrochemical oxidation signal of electro-active Tyrosine residues found in these proteins.[51−53] An indirect method to monitor the amyloid aggregation has also been developed in our laboratory using benzothiazole dyes, which had specific affinity to β-sheet structures.[54] In this report, a novel approach to the electrochemical and LSPR-based detection of αS aggregation is demonstrated using Au-ITO with the well-described interaction of αS with EGCG and Cu(II) ions. The effects of Cu(II) and EGCG on immobilized αS oligomers were detected using the redox probe $[Fe(CN)_6]^{3-/4-}$ in connection with cyclic voltammetry (CV) and differential pulse voltammetry (DPV).

Our electrochemical and LSPR measurements were confirmed using conventional Thioflavin-T (ThT) fluorescence, SPR imaging, and transmission electron microscopy (TEM) studies. Electrochemical and LSPR-based analyses of proteins on surfaces can be critical techniques to understand and provide insight into the effects of metals and small molecules on proteins. The label-free approach, nanofabrication, and mass production capabilities, together with the quick response time, may aid in the high-throughput screening of therapeutic candidates for PD.

MATERIALS AND METHODS

Chemicals and Reagents. Recombinant human α-synuclein (αS) was purchased from Anaspec Inc. (Fremont, CA). Thioflavin-T (ThT, 4-(3,6-dimethyl-1,3-benzothiazol-3-ium-2-yl)-*N*,*N*-dimethylaniline chloride; ∼75%), 11-unmercaptodecanol (MU), sodium phosphate monobasic (NaH_2PO_4; 99.0%), sodium phosphate dibasic (Na_2HPO_4; 99.0%), sodium bicarbonate ($NaHCO_3$), copper(II) chloride, 3,3′-dithiobios (sulfosuccinimidil-propionate) (DTSSP), sodium dodecyl sulfate (SDS), and epigallocatechin gallate (EGCG) were purchased from Sigma-Aldrich (Oakville, ON). Hydrogen peroxide (30% v/v) was obtained from EMD Inc., (Mississauga, ON). Polystyrene microspheres (10% w/w, 1.00 μm i.d.) were purchased from ThermoScientific Co. (Mississauga, ON). All samples were of analytical grade and prepared in phosphate buffered saline (50 mM, PBS), with 100 mM NaCl at pH 7.4 using 18.2 MΩ ultrapure water obtained from a Cascada LS water purification system (Pall Co., Mississauga, ON), unless stated otherwise.

Fabrication of Au-ITO Surfaces. Au-ITO surfaces were fabricated following a previously described protocol.[55,56] Briefly, ITO glass substrates were sonicated in acetone for 5 min followed by cleaning with copious amounts of water several times. ITO substrates were then sonicated in a 5:1:1 mixture of ammonium hydroxide/hydrogen peroxide/ultrapure water for 1 h before the glass substrates were further sonicated for 15 min in water. Polystyrene beads of 1 μm were equilibrated to room temperature before an aliquot (30 μL) was mixed with 100% (v/v) ethanol in a 1:1 ratio. An aliquot (20 μL) was then deposited on the dried ITO surface before immediately introducing it to the air−water interface of a Petri-dish filled with ultrapure water. ITO glass floated on the air−water interface as the solution spread out. After the microsphere solution was dispersed, a drop of 2% (w/v) SDS solution in water was added to the substrate to promote the formation of an ordered monolayer. ITO substrate was then left to dry. After samples were dried, 3 nm of Ti and 30 or 400 nm of Au were deposited using an electron beam evaporator (Hoser, Ottawa, ON). The beads were then removed by sonicating the samples in ethanol for about a minute before drying with nitrogen (Scheme S1, Supporting Information).

Electrochemistry. Electrochemical analysis was performed using a PGSTAT302N Metrohm Autolab potentiostat (Metrohm, Switzerland) and operated with the General Purpose Electrochemistry

DOI: 10.1021/am507972b
ACS Appl. Mater. Interfaces 2015, 7, 4081−4088

Scheme 1. Illustrative Representation of αS Immobilization onto Au-Nanopyramids on ITO Surfaces[a]

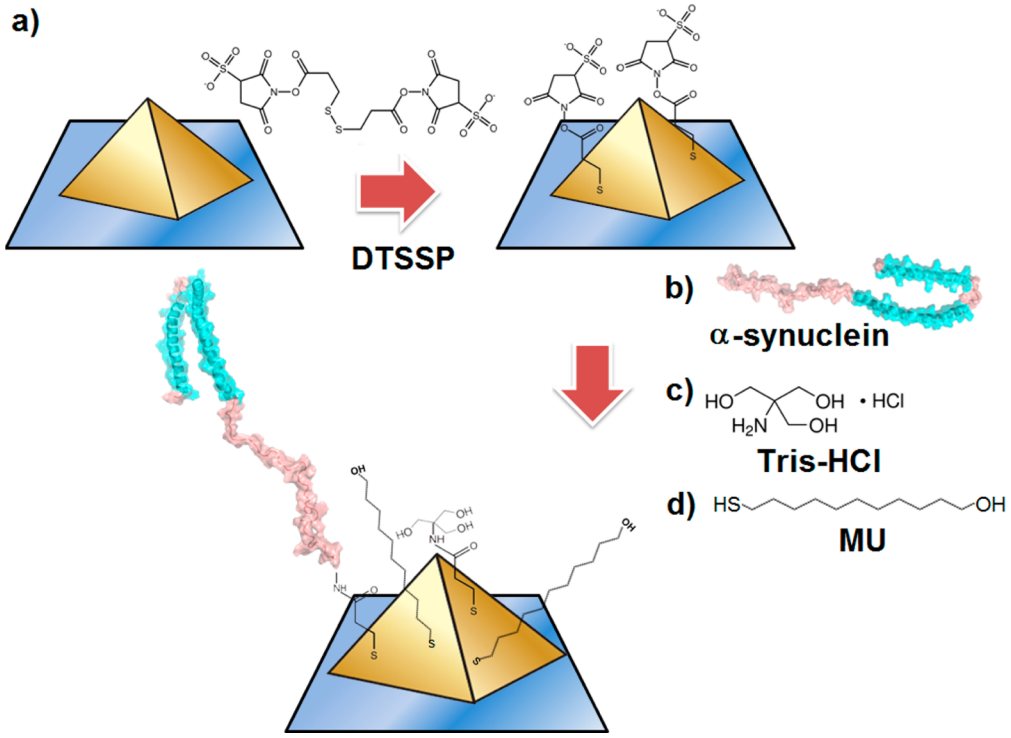

[a](a) DTSSP was immobilized as a linker for the covalent attachment of (b) αS. The unmodified DTSSP was quenched using (c) Tris-HCl, and the pinholes on the Au-nanopyramids were backfilled using (d) MU. Other conditions were as described in the Materials and Methods Section.

Software (GPES). The Au-ITO surface was activated using 2 mM DTSSP in 100 mM Na_2CO_3 (pH 8.5) by leaving it overnight at 4 °C.[57] Unbound DTSSP was later removed by stringent rinsing with water. After the immobilization of 10 μM αS oligomers in a droplet of 35 μL overnight, the unreacted DTSSP groups on the surface were blocked by incubating with 100 mM Tris-HCl (pH 7.5) at room temperature for 1 h. Backfilling of the noncoated Au surfaces was achieved by the immobilization of 1 mM MU (in 40% (v/v) ethanol) for 10 min, followed by ethanol rinsing (Scheme 1). Aliquots (20 μL) of 50 μM EGCG and Cu(II) were applied to the predetermined spots on the chip surface and allowed to incubate over 48 h, while electrochemical measurements were intermittently performed. Control experiments were also performed by incubating EGCG and Cu(II) on solely MU-modified surfaces to determine the nonspecific adsorption of those molecules.

CV and DPV measurements were performed using a three-electrode system that consisted of the Au-ITO surfaces as the working electrode, a leak-free miniature Ag/AgCl reference electrode (2 mm i.d., eDAQ Inc., Colorado Springs, CO), and a Pt wire as the counter electrode. An aliquot (35 μL) of 10 mM $[Fe(CN)_6]^{3-/4-}$ solution was dispensed onto the predetermined spots on the surface. CV measurements were taken at various scan rates from −0.25 to 0.65 V (vs Ag/AgCl). DPV was performed under the step potential of 5 mV with an amplitude of 50 mV. The nanostructured surfaces were stored in a fridge at 4 °C for 14 days, while CV measurements were intermittently performed at the various scan rates (10, 25, 50, 100, 250, and 500 mV/s) to monitor the changes in the electrochemical characteristics of the surfaces over time. Raw voltammograms were treated with Savitzky-Golay smoothing and baseline correction with a moving average peak width of 4 mV. All measurements were repeated ($n \geq 3$) to ensure statistical relevance.

Localized Surface Plasmon Resonance (LSPR). The optical system was composed of a spectrophotometer (USB-4000-UV−vis), a tungsten halogen light source (LS-1-LL, wavelength range of 200−1100 nm), a microfiber probe bundle (fiber core diameter of 400 μm, wavelength range of 300−1100 nm), and WS-1 diffuse reflectance standard, that were obtained from Ocean Optics (Dunedin, USA). The diffuse reflectance standard was used as a Lambertian reference surface. The microfiber probe was placed close to the working electrode surface so that incident light was reflected upon hitting the surface and then backed in the detector situated in the light probe. The absorbance mode of the Spectra Suite software was used to measure the spectral characteristics of the samples using 400 nm Au-pyramid coated ITO surfaces. The intensity and wavelengths of spectral peaks were recorded as modifications were made to the surfaces. The probe height was held constant (∼1 mm above the sample surface) throughout the study. All experiments were performed at room temperature (23 ± 2 °C).

ThT Fluorescence. The stock solution of 10 mM ThT was prepared in 18.2 MΩ water and protected from light. Fluorescence measurements were conducted in 96-well plates (BD Biosciences, Mississauga, ON) using a Synergy HT Multimode Microplate reader (BioTek, Winooski, VT). Each sample well contained: 50 μM ThT and 10 μM αS in the presence or absence of Cu(II) and EGCG (50 μM each). All experimental conditions were repeated in triplicate (n = 3). Control experiments were also performed for each condition. Results were normalized with their respective control fluorescence values to prevent any complications from the quenching of fluorescence by the small molecules. Spontaneous aggregation of αS samples was induced by incubation at 37 ± 1 °C with shaking at 300 rpm. Fluorescence (λ_{ex} 440 nm, λ_{em} 485 nm) was recorded at various time intervals for over ∼10 days.

Surface Plasmon Resonance Imaging (SPRi). αS samples were incubated at 37 °C for 6 days to form oligomers (as confirmed by ThT and TEM studies). Au spots of an SPRi array (GWC SpotReady-16 chip) were activated using 2 mM DTSSP that was deposited onto Au spots and left overnight at 4 °C. Nonspecifically adsorbed DTSSP was later removed by rinsing with water. After the immobilization of 10 μM αS overnight, the unreacted functional groups were blocked using 100 mM Tris-HCl (pH 7.5) incubated at room temperature for 1 h. Additional blocking of exposed Au surfaces was achieved by incubating with MU as described for the Au-ITO surfaces before. Control experiments were performed on five Au spots (processed with all

DOI: 10.1021/am507972b
ACS Appl. Mater. Interfaces 2015, 7, 4081−4088

previous steps except the protein immobilization). Finally, the SPRi array was mounted in the SPR imager-II system (GWC Technologies, Madison, WI). The SPRi-based detection principals were described in detail in our previous work.[35] In brief, p-polarized light, passing through a prism, was used to illuminate the Au surfaces at a fixed incident angle slightly smaller than the SPR angle. The reflected light then passed through a narrow band-pass filter centered at 830 nm and was collected using a CCD camera in connection with V++ 4.0 (Digital Optics, NZ). All the experiments were measured at 37 °C. The Au array was located inside the sealed flow cell, through which EGCG solution was circulated at varying concentrations at a flow rate of 100 μL/min. A PBS wash was performed after EGCG exposure to remove nonspecific binding. The increase in pixel intensity was then observed as a difference image. After converting to % reflectivity, the signals were plotted on a graph against time. The changes in reflectivity of all spots were normalized with the Au control spots on the array to account for the nonspecific binding events. SPR data was analyzed using the Langmuir model in customized software (GWC Technologies, Madison, WI).

Transmission Electron Microscopy (TEM). An aliquot (6 μL) of 10 μM αS oligomers was spotted onto nickel Formvar mesh grids (Electron Microscopy Sciences, Hatfield, PA) for 1 min and blotted dry. TEM grids were subsequently stained using 6 μL of 1% uranyl acetate for 1 min followed by blot drying. Samples were imaged using a Hitachi H-7500 TEM, which was operated at a range between 2 and 200 kV depending on the magnification required. Similar imaging experiments were performed using the αS oligomers that were exposed to 50 μM Cu(II) and EGCG after 48 h of incubation.

Scanning Electron Microscopy (SEM). A thin layer of Os was deposited, and the samples were imaged using an SEM system (LEO Zeiss 1530, Oberkochen, Germany). The electron gun voltage was set at 5.0 kV, and the software used to view the SEM images was Quartz PCI (Quartz Imaging Corp., Vancouver, BC). SEM of microspheres on ITO surfaces was performed using a Hitachi S530 scanning electron microscope (Hitachi, Japan). All ITO surfaces were sputtered with Au using the SEM coating unit PS3 (Agar Scientific, Essex, UK) at 19 mA plasma current for 100 s. The Au-ITO surfaces were then electrically connected to the sample stub by smearing silver paste dissolved in acetone from the sample to the metallic stub. The surface was observed at an acceleration voltage of 20 kV with a working distance of 5.0 mm.

RESULTS AND DISCUSSION

Initially, the interaction of αS oligomers with EGCG and Cu(II) was monitored using electrochemistry on Au-ITO surfaces. We hypothesized that the covalent immobilization of αS on the Au nanopyramids provided a large surface and flexibility for the dynamic aggregation of fibrils, while suppressing the steric hindrance. Using NSL on ITO surfaces, nanostructures resembling triangles were fabricated by depositing a 30 nm thick layer of Au (Figure 1A). When a 400 nm thick layer of Au was deposited on the surface, due to the large curvature of the polystyrene beads (inset of Figure 1B), the resulting shapes of the deposited Au resembled pyramid-like nanostructures (Figure 1B). When the Au-nanostructured ITO surfaces were used as a working electrode in CV measurements, the anodic and cathodic peaks appeared at approximately +0.27 and −0.15 V (vs Ag/AgCl), respectively. The contribution of Au nanostructures to increase the electro-active surface area was studied using CV (Figure 2) and DPV (Figure S1, Supporting Information). A significant increase in current signal was observed using the Au-nanopyramid modified ITO electrodes. From the DPV analysis, the relative increases in current signal for nanopyramid- and nanotriangle-modified ITO surfaces were determined as 26.6 ± 5.5% and 3.9 ± 1.3%, respectively. These results were attributed to the significantly larger electro-active surface area available on the nanopyramids as compared to the nanotriangles. Besides providing a larger electro-active surface area, the Au-nanopyramid modified ITO (Au-ITO) also allowed more space for the immobilization of thiolated molecules. Thus, Au-ITO surfaces were utilized for subsequent measurements.

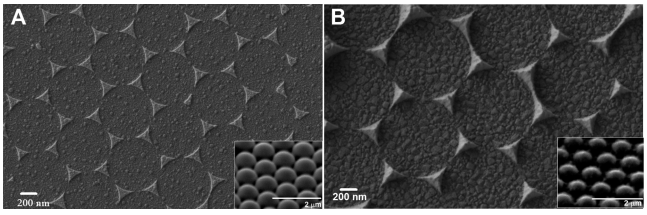

Figure 1. SEM images of (A) Au-nanotriangles and (B) Au-nanopyramids fabricated using NSL at 20 000× and 30 000× magnification, respectively. Inset depicts the SEM of nanospheres taken at a 45° angle before removal by sonication. Other conditions were as described in the Materials and Methods section.

Incubation of αS at 37 °C with shaking for 6 days promoted the formation of oligomeric species as described by Danzer et al.[26] After activating the Au-ITO surfaces with DTSSP, the oligomers were spotted on the chip surface for covalent immobilization, followed by the quenching of the remaining functional groups using Tris-HCl as described in the Materials and Methods section. Uncoated Au surfaces were also blocked by incubating with MU. After these modifications, a 55.8 ± 12.3% decrease in current signal was observed (Figure 3A,B). This implied that the protein and blocking layer contributed a significant resistance to the diffusion of $[Fe(CN)_6]^{3-/4-}$ to the electrode surface. CV at varying scan rates was performed as shown in Figure S2, Supporting Information. The inset of Figure S2, Supporting Information, shows the plot of peak current (i) vs $(\text{scan rate})^{1/2}$. The linear correlation demonstrated the reversible and diffusion-controlled characteristics of the redox processes on Au-ITO surfaces. A stability experiment was also performed over 2 weeks to ensure that the current signal did not fluctuate over time. Figure S3, Supporting Information, shows that the CV characteristics were similar within ∼5% error over time.

Cu(II) and EGCG were also individually incubated with the protein immobilized Au-ITO surfaces for 48 h to determine their effects on αS aggregation kinetics. As shown in Figure 3C, in the presence of EGCG, the current signal decreased over time, while in the presence of Cu(II), the current signal increased. Control experiments, that were performed in the absence of αS, displayed negligible current signal changes over time (not shown), indicating that the changes in current were not contributed by nonspecifically adsorbed Cu(II) or EGCG on the surfaces. The electrochemical results were in agreement with the TEM images (Figure S4, Supporting Information). TEM images were taken to observe αS aggregation in 20% (v/v) ethanol (Figure S4A,B, Supporting Information). We observed that, after 2 days of incubation, short nuclei of about ∼50−100 nm were formed, and in 6 days, oligomeric forms of αS were formed. The αS oligomers were up to several μm in length, collectively forming a mesh-network. Since previous reports indicated that αS aggregation was a seed/nucleation-dependent process,[58,59] the strand-like structures might have elongated from the ends of the short aggregates (formed in 2 days). After incubating the αS oligomers with Cu(II) for 48 h, a more compact network was formed (Figure S4C, Supporting Information). On the other hand, when

DOI: 10.1021/am507972b
ACS Appl. Mater. Interfaces 2015, 7, 4081−4088

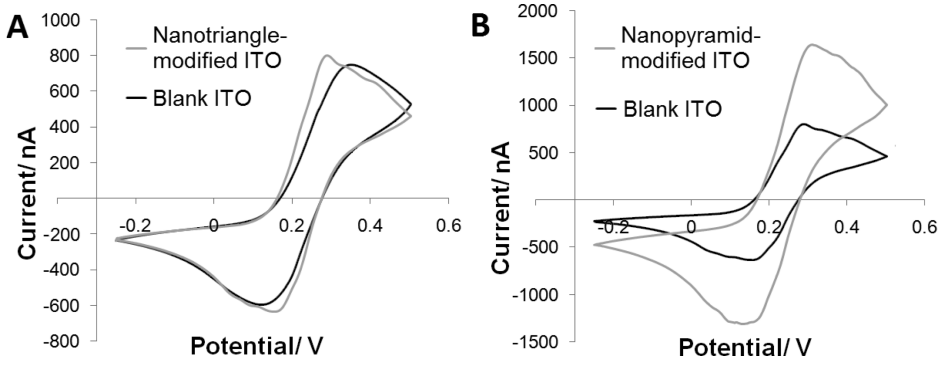

Figure 2. Cyclic voltammograms of 10 mM $[Fe(CN)_6]^{3-/4-}$ at (A) nanotriangle-modified ITO (gray line) and (B) nanopyramid-modified ITO (gray line) electrodes at a scan rate of 50 mV/s. Black line displays the CV response recorded for the blank ITO electrodes before Au nanostructure modification. Other conditions were as described in the Materials and Methods section.

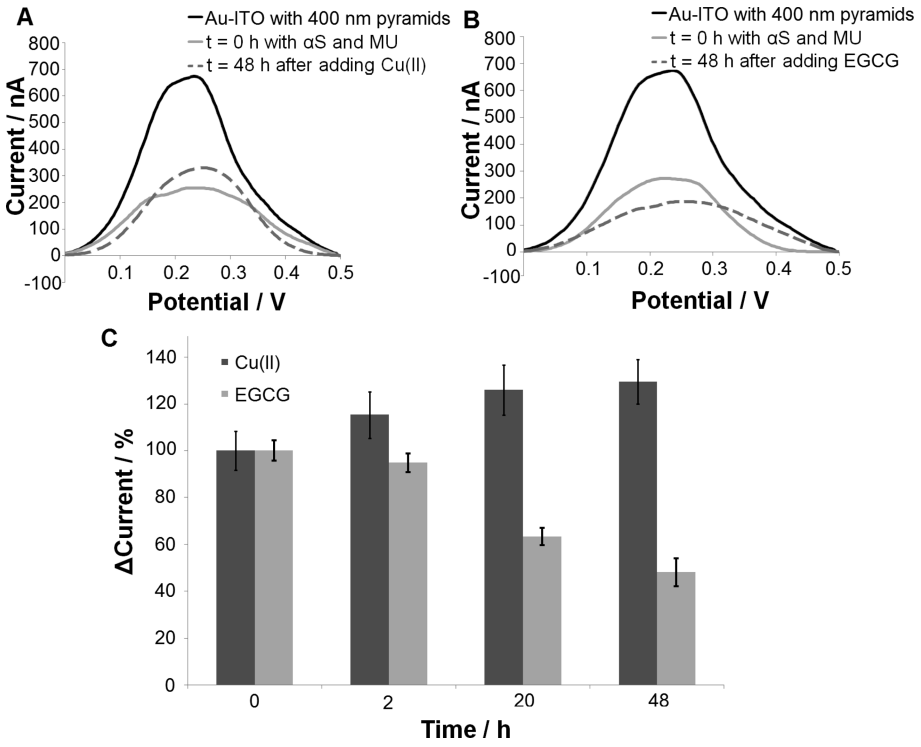

Figure 3. Representative differential pulse voltammograms of αS-immobilized Au-ITO surfaces, displaying the effect of (A) Cu(II) and (B) EGCG incubation on the anodic peak current signals at t = 48 h. (C) Electrochemical analysis of EGCG and metal interactions with αS oligomers showing a time dependence study of DPV anodic peak current of 10 mM $[Fe(CN)_6]^{3-/4-}$ after incubating 50 μM EGCG (light gray) and Cu(II) (dark gray) on corresponding immobilized αS oligomers on Au-ITO surfaces. Other conditions were as described in the Materials and Methods section.

EGCG was incubated with αS oligomers for 48 h, we observed the formation of optically dense amorphous aggregates (Figure S4D, Supporting Information), that were similar to those formed in our previous report about amyloid-β peptides.[45] Natalello and co-workers[38] reported that Cu(II) binding to αS induced extensive structural rearrangement of the protein, where αS was found in a highly compact state. We hypothesized that the dynamic rearrangement of αS oligomers into compact fibrils could have induced an increase in current signal by exposing more electro-active surface enabling the diffusion of $[Fe(CN)_6]^{3-/4-}$ to the surface. There may also be important effects of metal binding on the enhanced electro-activity on Au-ITOs. Since Cu(II) binds tightly to αS, the presence of metals embedded in the αS fibrils could have facilitated the charge transport to the Au-ITO surface.

The Au nanostructured surface had a uniformly periodic pattern, thus generating an LSPR effect upon excitation by light. The surface showed an LSPR absorbance peak at about 606 ± 0.6 nm with 0.446 ± 0.008 au in intensity (Figure 4A). Au-ITO surfaces modified with αS, MU, and EGCG were utilized for LSPR measurements (Figure 4B). The LSPR peak intensities and associated λ_{lspr} increased with the addition of αS and MU layers. Formation of these layers altered the electron density of the Au nanostructures, which then directly affect the surface plasmon absorption band and caused a bathochromic shift. Upon the interaction of EGCG with αS on the surface, the absorption of the plasmon mode increased and displayed a further bathochromic shift of 10−15 nm. This was in agreement with previous LSPR-based studies[60,61] and electrochemical data that supported the potential of using Au-nanopyramid coated ITO surfaces for future LSPR applications.

DOI: 10.1021/am507972b
ACS Appl. Mater. Interfaces 2015, 7, 4081−4088

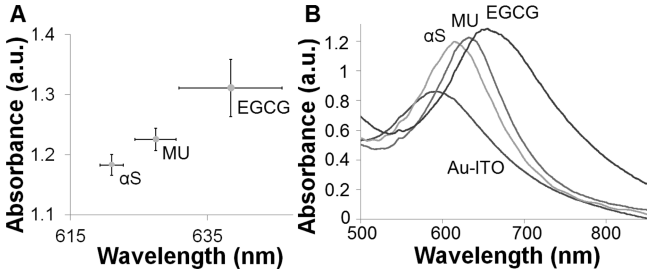

Figure 4. (A) Plot for the variations in LSPR absorption band peak wavelengths and intensities. (B) LSPR spectra observed on 400 nm pyramid Au-ITO surfaces as different target biomolecules interacted with αS. Other conditions were as described in the Materials and Methods section.

The shift in LSPR peak before and after the interaction of EGCG with the immobilized αS corresponded to the different morphological structures of the protein as shown in Figure S4B,D, respectively, Supporting Information. This nondestructive and simple qualitative LSPR measurement could serve as a quick confirmation for the binding of biomolecules to the substrate surface. It would require further NSL optimization in terms of the Au-nanopyramid height, size, and density to obtain a high FOM for our LSPR sensor. Further concentration dependence studies are in progress in our laboratory to obtain quantitative information on the interaction of biomolecules with αS.

In order to support our electrochemical and LSPR data, the aggregation of αS in the presence of Cu(II) and EGCG was analyzed using the well-described ThT fluorescence assay (Figure 5).[62] The several orders of magnitude increase in ThT

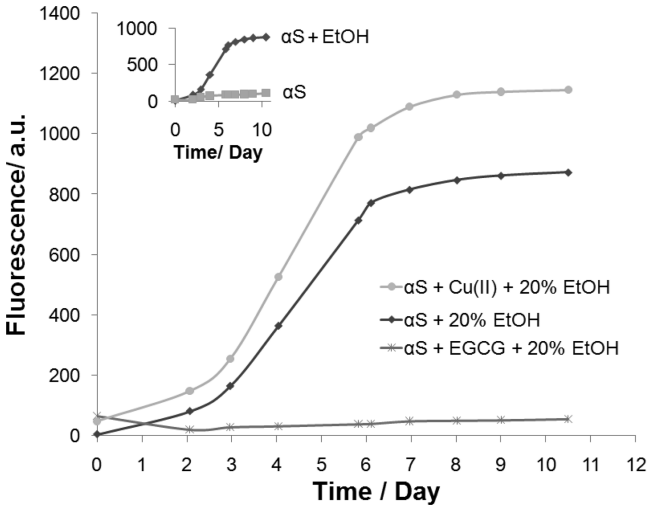

Figure 5. Average relative fluorescence intensity of ThT incubated with 10 μM αS and 20% ethanol monitored over 10 days in the presence and absence of 50 μM Cu(II) and EGCG. Triplicate measurements were performed for each sample (n = 3), and error bars were less than 50 au (not shown). Other conditions were as described in the Materials and Methods section.

fluorescence intensity upon fibril-binding makes it an especially sensitive indicator to detect the formation of β-sheets.[63] Following the protocol by Danzer et al.,[26] the polypeptide was incubated in the presence and absence of 20% ethanol with perturbation by shaking at 300 rpm in order to produce αS oligomers. The oligomeric forms of αS were used in this report, as they were reported to be the toxic species leading to neuronal death.[30] It was found that αS, in the presence of ethanol, significantly promoted aggregation and increased ThT fluorescence over ∼10 days; the signal increase was more than 10-fold smaller in the absence of ethanol (inset of Figure 5). The increase in ThT fluorescence induced by the formation of β-sheets reached a plateau in ∼7 days, in agreement with a previous report.[26] Cu(II) and EGCG were also separately incubated with oligomeric αS in the presence of ethanol. It was observed that αS incubated in the presence of Cu(II) displayed higher ThT fluorescence as compared to the αS alone (Figure 5), indicating that Cu(II) promoted the formation of β-sheets. This was consistent with the comparable ThT studies performed in the absence of ethanol (Figure S5, Supporting Information), as well as in the previous literature that reported the acceleration effect of Cu(II) on αS aggregation.[31,64−66] In the presence of EGCG, the formation of αS fibrils was suppressed as observed from negligible ThT fluorescence (under 60 au) recorded in over 10 days, indicating that the amorphous aggregates observed in TEM did not contain β-sheets. The low ThT fluorescence indicated that unstructured aggregates were formed.[44,47] We have also shown in our previous report[45] that there was negligible influence of EGCG on ThT fluorescence in the presence of amyloid-β peptides related to AD.

To verify the formation of αS-EGCG complexes on surfaces, SPRi studies were also performed. The binding affinity of EGCG was determined using αS oligomers that were formed in 6 days of incubation. αS oligomers were first immobilized on the Au surfaces of the array using the DTSSP-based method as described in the Materials and Methods section. EGCG samples at varying concentrations were then exposed to the array at a flow rate of 100 μL/min. As the EGCG interacted with the immobilized αS, the reflectivity ratio increased, as shown in Figure S6, Supporting Information. After ∼150 s, PBS buffer was flown across the chip surface to remove nonspecifically bound EGCG, causing a drop in the reflectivity ratio. Using the Langmuir model to fit the different concentration curves (inset of Figure S6, Supporting Information), the equilibrium dissociation constant, K_D, between EGCG and αS oligomers was calculated to be 2.71 ± 0.54 μM. A similarly strong affinity between EGCG and αS was also observed by Bieschke et al.[44] in their recently published report.

CONCLUSIONS

We demonstrated the preliminary data from a promising dual detection platform for monitoring the morphological changes of αS oligomers upon small molecule interactions using electrochemistry and LSPR. The changes in the structure of αS oligomers were manifested as fluctuations in DPV peak current and LSPR absorption band signals. To the best of our knowledge, this was a novel attempt to monitor structural changes of immobilized αS oligomers by following the changes in the well-described electrochemical properties of $[Fe(CN)_6]^{3-/4-}$. Our preliminary electrochemical and LSPR results were complemented by established techniques for the detection of protein misfolding. ThT fluorescence and TEM imaging studies suggested that dense and unstructured amorphous αS aggregates were induced by EGCG, while β-sheet-rich and compact αS mesh-networks were promoted by Cu(II) ions. SPRi studies also confirmed the strong binding affinity of EGCG to αS aggregates on Au surfaces. The reported electrochemical system is a promising platform for the low-cost

DOI: 10.1021/am507972b
ACS Appl. Mater. Interfaces 2015, 7, 4081−4088

and high-throughput screening of small drug candidates that target αS and will accelerate the drug discovery efforts toward the therapy of PD.

■ ASSOCIATED CONTENT

Supporting Information

Differential pulse voltammetry of different Au nanostructured surfaces; scan rate dependence of anodic peak current; electrochemical stability of the αS-immobilized Au-ITO surface; transmission electron micrographs of αS before and after interacting with modulators; Thioflavin-T fluorescence assay of αS and modulators; surface plasmon resonance imaging analysis of the interaction between EGCG and αS. This material is available free of charge via the Internet at http://pubs.acs.org.

■ AUTHOR INFORMATION

Corresponding Author

*Tel: +1 416 287 7249. Fax: +1 416 287 7279. E-mail: kagan.kerman@utoronto.ca.

Notes

The authors declare no competing financial interest.

■ ACKNOWLEDGMENTS

The authors gratefully acknowledge the financial support from the Biomedical Young Investigator Award of the Alzheimer Society of Canada and NSERC Discovery Grant. We also appreciate the help of Brandon Bernal and Vithien Nguyen for performing some of the experiments. F.L.-L. acknowledges the Western Nanofabrication Facility and the Canada Research Chair program.

■ REFERENCES

(1) Haynes, C. L.; Van Duyne, R. P. Nanosphere Lithography: A Versatile Nanofabrication Tool for Studies of Size-Dependent Nanoparticle Optics. *J. Phys. Chem. B* **2001**, *105*, 5599−5611.

(2) Tabatabaei, M.; Sangar, A.; Kazemi-Zanjani, N.; Torchio, P.; Merlen, A.; Lagugné-Labarthet, F. Optical Properties of Silver and Gold Tetrahedral Nanopyramid Arrays Prepared by Nanosphere Lithography. *J. Phys. Chem. C* **2013**, *117*, 14778−14786.

(3) Zhao, J.; Zhang, X.; Yonzon, C. R.; Haes, A. J.; Van Duyne, R. P. Localized Surface Plasmon Resonance Biosensors. *Nanomedicine* **2006**, *1*, 219−228.

(4) Fayyaz, S.; Tabatabaei, M.; Hou, R.; Lagugné-Labarthet, F. Surface-Enhanced Fluorescence: Mapping Individual Hot Spots in Silica-Protected 2D Gold Nanotriangle Arrays. *J. Phys. Chem. C* **2012**, *116*, 11665−11670.

(5) Zhang, X.; Hicks, E. M.; Zhao, J.; Schatz, G. C.; Van Duyne, R. P. Electrochemical Tuning of Silver Nanoparticles Fabricated by Nanosphere Lithography. *Nano Lett.* **2005**, *5*, 1503−1507.

(6) Yu, J.; Yan, Q.; Shen, D. Co-Self-Assembly of Binary Colloidal Crystals at the Air−Water Interface. *ACS Appl. Mater. Interfaces* **2010**, *2*, 1922−1926.

(7) Haynes, C. L.; Van Duyne, R. P. Plasmon-Sampled Surface-Enhanced Raman Excitation Spectroscopy. *J. Phys. Chem. B* **2003**, *107*, 7426−7433.

(8) Marquestaut, N.; Martin, A.; Talaga, D.; Servant, L.; Ravaine, S.; Reculusa, S. P.; Bassani, D. M.; Gillies, E.; Lagugné-Labarthet, F. Raman Enhancement of Azobenzene Monolayers on Substrates Prepared by Langmuir−Blodgett Deposition and Electron-Beam Lithography Techniques. *Langmuir* **2008**, *24*, 11313−11321.

(9) Wallace, G. Q.; Tabatabaei, M.; Lagugné-Labarthet, F. Towards Attomolar Detection Using a Surface-Enhanced Raman Spectroscopy Platform Fabricated by Nanosphere Lithography. *Can. J. Chem.* **2013**, *92*, 1−8.

(10) Wang, H.; Brandl, D. W.; Le, F.; Nordlander, P.; Halas, N. J. Nanorice: A Hybrid Plasmonic Nanostructure. *Nano Lett.* **2006**, *6*, 827−832.

(11) Bukasov, R.; Shumaker-Parry, J. S. Highly Tunable Infrared Extinction Properties of Gold Nanocrescents. *Nano Lett.* **2007**, *7*, 1113−1118.

(12) Auguié, B.; Barnes, W. L. Collective Resonances in Gold Nanoparticle Arrays. *Phys. Rev. Lett.* **2008**, *101*, 143902.

(13) Vecchi, G.; Giannini, V.; Gómez Rivas, J. Surface Modes in Plasmonic Crystals Induced by Diffractive Coupling of Nanoantennas. *Phys. Rev. B* **2009**, *80*, 201401(R).

(14) Zhou, W.; Odom, T. W. Tunable Subradiant Lattice Plasmons by Out-of-Plane Dipolar Interactions. *Nat. Nanotechnol.* **2011**, *6*, 423−427.

(15) Shen, Y.; Zhou, J.; Liu, T.; Tao, Y.; Jiang, R.; Liu, M.; Xiao, G.; Zhu, J.; Zhou, Z.-K.; Wang, X.; Jin, C.; Wang, J. Plasmonic Gold Mushroom Arrays with Refractive Index Sensing Figures of Merit Approaching the Theoretical Limit. *Nat. Commun.* **2013**, *4*, 2381.

(16) Hutter, E.; Fendler, J. H. Exploitation of Localized Surface Plasmon Resonance. *Adv. Mater.* **2004**, *16*, 1685−1706.

(17) Sepúlveda, B.; Angelomé, P. C.; Lechuga, L. M.; Liz-Marzán, L. M. LSPR-Based Nanobiosensors. *Nano Today* **2009**, *4*, 244−251.

(18) Bansal, A.; Verma, S. S. Optical Response of Noble Metal Alloy Nanostructures. *Phys. Lett. A* **2015**, *379*, 163−169.

(19) Colson, P.; Hentist, C.; Cloots, R. Nanosphere Lithography: A Powerful Method for the Controlled Manufacturing of Nanomaterials. *J. Nanomater.* **2013**, *2013*, 948510.

(20) Zhang, D.; Lu, Y.; Jiang, J.; Zhang, Q.; Yao, Y.; Wang, P.; Chen, B.; Cheng, Q.; Liu, G. L.; Liu, Q. Nanoplasmonic Biosensor: Coupling Electrochemistry to Localized Surface Plasmon Resonance Spectroscopy on Nanocup Arrays. *Biosens. Bioelectron.* **2014**, DOI: 10.1016/j.bios.2014.08.022.

(21) Endo, T.; Takizawa, H.; Yanagida, Y.; Hatsuzawa, T.; Tamiya, E. Construction of a Biosensor Operating on the Combined Principles of Electrochemical Analysis and Localized Surface Plasmon Resonance for Multiple Detection of Antigen-Antibody and Enzymatic Reactions on the Single Biosensor. *Sens. Mater.* **2008**, *20*, 255−265.

(22) Eriksen, J.; Wszolek, Z.; Petrucelli, L. Molecular Pathogenesis of Parkinson Disease. *Arch. Neurol.* **2005**, *62*, 353−357.

(23) Bryan, T.; Luo, X.; Forsgren, L.; Morozova-Roche, L. A.; Davis, J. J. The Robust Electrochemical Detection of a Parkinson's Disease Marker in Whole Blood Sera. *Chem. Sci.* **2012**, *3*, 3468−3473.

(24) Liu, S.; Ninan, I.; Antonova, I.; Battaglia, F.; Trinchese, F.; Narasanna, A.; Kolodilov, N.; Dauer, W.; Hawkins, R. D.; Arancio, O. [alpha]-Synuclein Produces a Long-Lasting Increase in Neurotransmitter Release. *EMBO J.* **2004**, *23*, 4506−4516.

(25) Dauer, W.; Przedborski, S. Parkinson's Disease: Mechanisms and Models. *Neuron* **2003**, *39*, 889−909.

(26) Danzer, K. M.; Haasen, D.; Karow, A. R.; Moussaud, S.; Habeck, M.; Giese, A.; Kretzschmar, H.; Hengerer, B.; Kostka, M. Different Species of α-Synuclein Oligomers Induce Calcium Influx and Seeding. *J. Neurosci.* **2007**, *27*, 9220−9232.

(27) Lundvig, D.; Lindersson, E.; Jensen, P. H. Pathogenic Effects of α-Synuclein Aggregation. *Mol. Brain Res.* **2005**, *134*, 3−17.

(28) Bennett, M. C. The Role of α-Synuclein in Neurodegenerative Diseases. *Pharmacol. Ther.* **2005**, *105*, 311−331.

(29) Conway, K. A.; Lee, S.-J.; Rochet, J.-C.; Ding, T. T.; Williamson, R. E.; Lansbury, P. T. Acceleration of Oligomerization, not Fibrillization, Is a Shared Property of Both α-Synuclein Mutations Linked to Early-Onset Parkinson's Disease: Implications for Pathogenesis and Therapy. *Proc. Natl. Acad. Sci. U.S.A.* **2000**, *97*, 571−576.

(30) Wright, J. A.; Wang, X.; Brown, D. R. Unique Copper-Induced Oligomers Mediate Alpha-Synuclein Toxicity. *FASEB J.* **2009**, *23*, 2384−2393.

(31) Uversky, V. N. A Protein-Chameleon: Conformational Plasticity of α-Synuclein, a Disordered Protein Involved in Neurodegenerative Disorders. *J. Biomol. Struct. Dyn.* **2003**, *21*, 211−234.

(32) El-Agnaf, O. M. A.; Salem, S. A.; Paleologou, K. E.; Curran, M. D.; Gibson, M. J.; Court, J. A.; Schlossmacher, M. G.; Allsop, D.

DOI: 10.1021/am507972b
ACS Appl. Mater. Interfaces 2015, 7, 4081−4088

Detection of Oligomeric Forms of α-Synuclein Protein in Human Plasma as a Potential Biomarker for Parkinson's Disease. *FASEB J.* **2006**, *20*, 419−425.
(33) Sung, Y.-H.; Rospigliosi, C.; Eliezer, D. NMR Mapping of Copper Binding Sites in Alpha-Synuclein. *Biochim. Biophys. Acta* **2006**, *1764*, 5−12.
(34) Rasia, R. M.; Bertoncini, C. W.; Marsh, D.; Hoyer, W.; Cherny, D.; Zweckstetter, M.; Griesinger, C.; Jovin, T. M.; Fernández, C. O. Structural Characterization of Copper(II) Binding to α-Synuclein: Insights into the Bioinorganic Chemistry of Parkinson's Disease. *Proc. Natl. Acad. Sci. U.S.A.* **2005**, *102*, 4294−4299.
(35) Brown, D. R. Metal Binding to Alpha-Synuclein Peptides and Its Contribution to Toxicity. *Biochem. Biophys. Res. Commun.* **2009**, *380*, 377−381.
(36) Dexter, D. T.; Wells, F. R.; Lee, A. J.; Agid, F.; Agid, Y.; Jenner, P.; Marsden, C. D. Increased Nigral Iron Content and Alterations in Other Metal Ions Occurring in Brain in Parkinson's Disease. *J. Neurochem.* **1989**, *52*, 1830−1836.
(37) Sung, J. Y.; Kim, J.; Paik, S. R.; Park, J. H.; Ahn, Y. S.; Chung, K. C. Induction of Neuronal Cell Death by Rab5A-Dependent Endocytosis of α-Synuclein. *J. Biol. Chem.* **2001**, *276*, 27441−27448.
(38) Natalello, A.; Benetti, F.; Doglia, S. M.; Legname, G.; Grandori, R. Compact Conformations of α-Synuclein Induced by Alcohols and Copper. *Proteins* **2011**, *79*, 611−621.
(39) Hyung, S.-J.; DeToma, A. S.; Brender, J. R.; Lee, S.; Vivekanandan, S.; Kochi, A.; Choi, J.-S.; Ramamoorthy, A.; Ruotolo, B. T.; Lim, M. H. Insights into Antiamyloidogenic Properties of the Green Tea Extract (−)-Epigallocatechin-3-gallate toward Metal-Associated Amyloid-β Species. *Proc. Natl. Acad. Sci. U.S.A.* **2013**, *110*, 3743−3748.
(40) Ehrnhoefer, D. E.; Duennwald, M.; Markovic, P.; Wacker, J. L.; Engemann, S.; Roark, M.; Legleiter, J.; Marsh, J. L.; Thompson, L. M.; Lindquist, S.; Muchowski, P. J.; Wanker, E. E. Green tea (−)-Epigallocatechin-gallate Modulates Early Events in Huntingtin Misfolding and Reduces Toxicity in Huntington's Disease Models. *Hum. Mol. Genet.* **2006**, *15*, 2743−2751.
(41) Rambold, A. S.; Miesbauer, M.; Olschewski, D.; Seidel, R.; Riemer, C.; Smale, L.; Brumm, L.; Levy, M.; Gazit, E.; Oesterhelt, D.; Baier, M.; Becker, C. F. W.; Engelhard, M.; Winklhofer, K. F.; Tatzelt, J. Green Tea Extracts Interfere with the Stress-Protective Activity of PrPC and the Formation of PrPSc. *J. Neurochem.* **2008**, *107*, 218−229.
(42) Hauber, I.; Hohenberg, H.; Holstermann, B.; Hunstein, W.; Hauber, J. The Main Green Tea Polyphenol Epigallocatechin-3-gallate Counteracts Semen-Mediated Enhancement of HIV Infection. *Proc. Natl. Acad. Sci. U.S.A.* **2009**, *106*, 9033−9038.
(43) Roberts, B. E.; Duennwald, M. L.; Wang, H.; Chung, C.; Lopreiato, N. P.; Sweeny, E. A.; Knight, M. N.; Shorter, J. A Synergistic Small-Molecule Combination Directly Eradicates Diverse Prion Strain Structures. *Nat. Chem. Biol.* **2009**, *5*, 936−946.
(44) Bieschke, J.; Russ, J.; Friedrich, R. P.; Ehrnhoefer, D. E.; Wobst, H.; Neugebauer, K.; Wanker, E. E. EGCG Remodels Mature Alpha-synuclein and Amyloid-beta Fibrils and Reduces Cellular Toxicity. *Proc. Natl. Acad. Sci. U.S.A.* **2010**, *107*, 7710−7715.
(45) Cheng, X. R.; Hau, B. Y. H.; Veloso, A. J.; Martic, S.; Kraatz, H.-B.; Kerman, K. Surface Plasmon Resonance Imaging of Amyloid-beta Aggregation Kinetics in the Presence of Epigallocatechin Gallate and Metals. *Anal. Chem.* **2012**, *85*, 2049−2055.
(46) Cheng, X. R.; Sze Hung, V. W.; Scarano, S.; Mascini, M.; Minunni, M.; Kerman, K. Label-Free Methods for Probing the Interaction of Clioquinol with Amyloid-beta. *Anal. Methods* **2012**, *4*, 2228−2232.
(47) Ehrnhoefer, D. E.; Bieschke, J.; Boeddrich, A.; Herbst, M.; Masino, L.; Lurz, R.; Engemann, S.; Pastore, A.; Wanker, E. E. EGCG Redirects Amyloidogenic Polypeptides into Unstructured, Off-Pathway Oligomers. *Nat. Struct. Mol. Biol.* **2008**, *15*, 558−566.
(48) Wang, X.; Moualla, D.; Wright, J. A.; Brown, D. R. Copper Binding Regulates Intracellular Alpha-synuclein Localisation, Aggregation and Toxicity. *J. Neurochem.* **2010**, *113*, 704−714.
(49) Quinn, S. D.; Dalgarno, P. A.; Cameron, R. T.; Hedley, G. J.; Hacker, C.; Lucocq, J. M.; Baillie, G. S.; Samuel, I. D. W.; Penedo, J. C. Real-Time Probing of [beta]-Amyloid Self-Assembly and Inhibition Using Fluorescence Self-Quenching between Neighbouring Dyes. *Mol. BioSyst.* **2014**, *10*, 34−44.
(50) Chandrashekaran, I. R.; Adda, C. G.; MacRaild, C. A.; Anders, R. F.; Norton, R. S. EGCG Disaggregates Amyloid-like Fibrils Formed by Plasmodium Falciparum Merozoite Surface Protein 2. *Arch. Biochem. Biophys.* **2011**, *513*, 153−157.
(51) Chan, T.; Chow, A. M.; Tang, D. W. F.; Li, Q.; Wang, X.; Brown, I. R.; Kerman, K. Interaction of Baicalein and Copper with α-Synuclein: Electrochemical Approach to Parkinson's Disease. *J. Electroanal. Chem.* **2010**, *648*, 151−155.
(52) Hung, V. W.-S.; Masoom, H.; Kerman, K. Label-Free Electrochemical Detection of Amyloid Beta Aggregation in the Presence of Iron, Copper and Zinc. *J. Electroanal. Chem.* **2012**, *681*, 89−95.
(53) Hung, V. W. S.; Cheng, X. R.; Li, N.; Veloso, A. J.; Kerman, K. Electrochemical Detection of Amyloid-Beta Aggregation in the Presence of Resveratrol. *J. Electrochem. Soc.* **2013**, *160*, G3097−G3101.
(54) Veloso, A. J.; Hung, V. W. S.; Sindhu, G.; Constantinof, A.; Kerman, K. Electrochemical Oxidation of Benzothiazole Dyes for Monitoring Amyloid Formation Related to the Alzheimer's Disease. *Anal. Chem.* **2009**, *81*, 9410−9415.
(55) Murray-Methot, M.-P.; Menegazzo, N.; Masson, J.-F. Analytical and Physical Optimization of Nanohole-Array Sensors Prepared by Modified Nanosphere Lithography. *Analyst* **2008**, *133*, 1714−1721.
(56) Huang, W.; Qian, W.; El-Sayed, M. A.; Ding, Y.; Wang, Z. L. Effect of the Lattice Crystallinity on the Electron-Phonon Relaxation Rates in Gold Nanoparticles. *J. Phys. Chem. C* **2007**, *111*, 10751−10757.
(57) Vallina-García, R.; del Mar García-Suárez, M.; Fernández-Abedul, M. T.; Méndez, F. J.; Costa-García, A. Oriented Immobilisation of Anti-pneumolysin Fab through a Histidine Tag for Electrochemical Immunosensors. *Biosens. Bioelectron.* **2007**, *23*, 210−217.
(58) Wood, S. J.; Wypych, J.; Steavenson, S.; Louis, J.-C.; Citron, M.; Biere, A. L. α-Synuclein Fibrillogenesis Is Nucleation-Dependent: Implications for the Pathogenesis of Parkinson's Disease. *J. Biol. Chem.* **1999**, *274*, 19509−19512.
(59) Kim, H. J.; Eri, C.; Yuji, G.; Seung, R. P. Seed-Dependent Accelerated Fibrillation of Alpha-Synuclein Induced by Periodic Ultrasonication Treatment. *J. Microbiol. Biotechnol.* **2007**, *17*, 2027−2032.
(60) Lin, Y.; Zou, Y.; Lindquist, R. G. A Reflection-Based Localized Surface Plasmon Resonance Fiber-Optic Probe for Biochemical Sensing. *Biomed. Opt. Express* **2011**, *2*, 478−484.
(61) Hsu, C.-Y.; Huang, J.-W.; Lin, K.-J. High Sensitivity and Selectivity of Human Antibody Attachment at the Interstices between Substrate-Bound Gold Nanoparticles. *Chem. Commun.* **2011**, *47*, 872−874.
(62) Levine, H. Thioflavine T Interaction with Synthetic Alzheimer's Disease Beta-Amyloid Peptides: Detection of Amyloid Aggregation in Solution. *Protein Sci.* **1993**, *2*, 404−410.
(63) Naiki, H.; Higuchi, K.; Nakakuki, K.; Takeda, T. Kinetic Analysis of Amyloid Fibril Polymerization in Vitro. *Lab. Invest.* **1991**, *65*, 104−110.
(64) Barnham, K. J.; Bush, A. I. Metals in Alzheimer's and Parkinson's Diseases. *Curr. Opin. Chem. Biol.* **2008**, *12*, 222−228.
(65) Bharathi; Rao, K. S. Molecular Understanding of Copper and Iron Interaction with α-Synuclein by Fluorescence Analysis. *J. Mol. Neurosci.* **2008**, *35*, 273−281.
(66) Biancalana, M.; Koide, S. Molecular Mechanism of Thioflavin-T Binding to Amyloid Fibrils. *Biochim. Biophys. Acta* **2010**, *1804*, 1405−1412.

DOI: 10.1021/am507972b
ACS Appl. Mater. Interfaces 2015, 7, 4081−4088